iScience

Article

Anti-smudge superhard transparent coatings via ultra-small nanoparticle pattern surfaces

Graphical abstract

Authors

Jieran Li, Xiubin Xu, Dian Lin, Yueyan Liang, Yashi Huang, Xu Wu

Correspondence

xuxb@gzhu.edu.cn (X.X.), xuwu@gzhu.edu.cn (X.W.)

In brief

Natural sciences; Applied sciences; Materials science

Highlights

- Anti-smudge coatings exhibited transparent and superhard properties
- A facile preparation was developed for anti-smudge coatings
- A conceptional nanoparticle pattern surface strategy was proposed
- The coating exhibited good adhesion on various substrates

Li et al., 2025, iScience *28*, 111996
March 21, 2025
https://doi.org/10.1016/j.isci.2025.111996

CellPress

iScience

CellPress
OPEN ACCESS

Article

Anti-smudge superhard transparent coatings via ultra-small nanoparticle pattern surfaces

Jieran Li,[1] Xiubin Xu,[1,2,*] Dian Lin,[1] Yueyan Liang,[1] Yashi Huang,[1] and Xu Wu[1,*]
[1]School of Chemistry and Chemical Engineering, Guangzhou University, Guangzhou 510006, P.R. China
[2]Lead contact
*Correspondence: xuxb@gzhu.edu.cn (X.X.), xuwu@gzhu.edu.cn (X.W.)
https://doi.org/10.1016/j.isci.2025.111996

SUMMARY

Anti-smudge coating materials have a broad prospect, but they are susceptible to wear from nails and sand. Therefore, the potential application of such coatings on glass substrates needs coating features such as superhardness and high transparency. However, realizing these key properties combined with anti-smudge function is significantly challenging. In this work, we show a conceptional nanoparticle pattern designing strategy of materials, inspired by stepping on cobblestone roads with the foot feeling of only the hardness of stones. Realize the nanoparticle pattern surface of "cobblestone roads" via facile and scalable interfacial reactions within a molecular compatible system, to successfully achieve the desired coating material properties including anti-smudge, superhardness, and high transparency. The coating was composed of tensely crosslinked sub-10 nm building blocks that bear an anti-smudge molecular layer, exhibiting undistinguished inorganic phase behavior when it was subjected to external forces within the contact point of micro- or above 10 nm nanoscale.

INTRODUCTION

Anti-smudge coatings with low-adhesive surfaces can protect substrates against both aqueous and oily contaminants, showing significant importance and promise for self-cleaning application scenarios.[1–6] Generally, the anti-smudge function of materials is achieved with low-surface-energy compounds enriched on the surfaces, such as fluorine- or silicon-based amphiphobic organic molecules or polymers.[7–11] The inherent softness of organic compositions makes materials with anti-smudge properties exhibit limited hardness, which are critical issues for the robustness of coating materials as well as the protection of various underlying substrates.[12–14] In practical applications, high hardness and transparency are important for the application of the coating, such as the coating used on screens of mobile phone screens, windows, and cars. The applied glass may face the wear of nails and sand, while the line of sight must be not affected during use. Furthermore, high hardness can prolong the coating's lifetime, avoiding abrasion during the application. Thus, high hardness and transparency of anti-fouling coatings are essential to fulfill the applicable requirements.

To improve hardness and scratch resistance, inorganic hard fillers have been incorporated into the anti-smudge organic coating materials.[15–18] However, these hybrid coating composites tend to have significant heterostructure, Young's modulus mismatch, and weak interfacial interaction between inorganic fillers and organic matrixes, thus typically resulting in only modest improvements in hardness. Moreover, these fillers, and various nanomaterials that were used to fabricate superamphiphobic surfaces[19–21] or SLIPS,[22] as well as the crystallinity of PTFE-based materials tend to scatter light, which can affect the transparency of these materials[23,24] with anti-smudge performance and render them unsuitable for applications as wearable electronics or windows. To the best of our knowledge, only polyhedral oligomeric silsesquioxane (POSS), with cage-like inorganic/organic hybrid structure, was reported to achieve both anti-smudge function and superhardness (above 9H, inorganic level), and the molecular scaled composition can avoid the light scattering induced opacity.[25–27] However, the complex preparation, low solubility in various solvents, and high price of POSS restrict its large-scale industrial production as well as the application of hard anti-smudge coatings in different fields.[28,29]

Inspired by stepping on cobblestone roads with the foot feeling of only the hardness of stones, herein, we proposed a conceptional strategy, a nanoparticle pattern surface based on ultra-small nanoparticles, to balance and guarantee the desired material properties including anti-smudge performance, superhardness, and transparency. Unlike the traditional method of choosing and integrating different organic/inorganic composites, our approach utilized interfacial reactions within a molecular compatible system, to realize the reduced-scale particle pattern of "cobblestone roads." The building blocks function as ultra-small "cobblestones" with a size of only several nanometers to form the superhard particle pattern surface. Thus, after the coating is crosslinked, the coating could show the cobblestones road-like particle surface properties and external factors cannot affect the crosslinked part of the particles, mimicking a cobblestone road where hard cobblestones are wrapped in cement and the surface only shows the nature of cobblestones. In

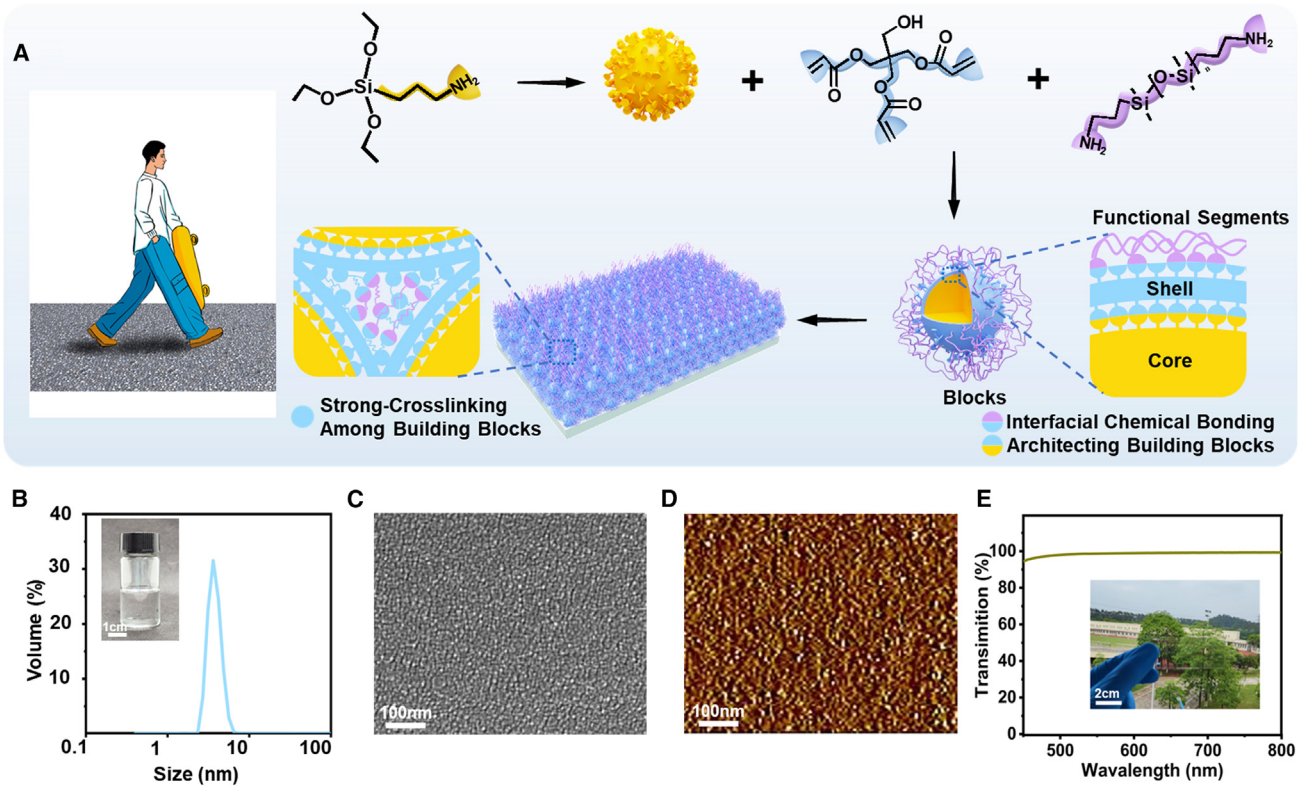

Figure 1. Preparation and transparency

(A) Illustration of the design and preparation of anti-smudge superhard transparent coating via "cobblestones road" nanoparticle pattern designing of materials.

(B) The size distribution of the building blocks, and the picture indicating the crystal clearness of the aqueous solution containing the building blocks.

(C and D) The SEM (C) and AFM (D) images of the coating surfaces, exhibiting the reduced-scale structures of cobblestone roads with a surface roughness (Ra: 0.441 nm).

(E) Transmittance spectra of the coating, with the inserted picture indicating the transparency of the coated glass.

addition, interfacial molecular engineering endowed the building blocks with highly crosslinkable and anti-smudge functional segments. The resulting clear solution can be easily sprayed, dipped, or painted on-site onto various objects, and subsequently obtain the desired superhard, anti-smudge, also transparent coating materials. These coatings use inorganic nanoparticles to cover surfaces with the highest hardness requirements to avoid the problem of insufficient hardness of organic components, and the resulting transparent solution can be easily sprayed impregnated or applied on-site to various objects (such as aluminum, iron, glass, and polytetrafluoroethylene). Thus, these coatings are promising for various applications, such as electronic touch screens, windows of vehicles or skyscrapers. We believe that the nanoparticle pattern surface strategy can be used for the fabrication of many materials including those that wish to achieve the combination of different organic and inorganic characteristics.

RESULTS AND DISCUSSION

Preparation and characterization of the coating

Our approach for preparing anti-smudge superhard transparent coatings is shown in Figure 1A. Specifically, the superhard organic core of building blocks bearing amino groups was initially prepared by the hydrolyzation of 3-aminopropyl triethoxysilane (APTES). Subsequently, the core can react with the double bonds of the pentaerythritol triacrylate (PETA) comprised shell via Michael addition. Similarly, the amino groups of amino-terminated polydimethylsiloxane (NH_2-PDMS-NH_2) can also react with PETA to impart the building blocks with anti-smudge properties, while the surplus double bonds of PETA would contribute to the highly crosslinking reaction among building blocks. These reactions resulted in a clear solution comprising the building blocks with the size primarily distributed between 1 and 10 nm (Figure 1B).

This solution is applicable for industrial coating techniques such as spraying and painting, and the final coating materials could be obtained after curing at 180°C for 2 h. As predicted, the homogeneous morphology of the tensely crosslinked building blocks, exhibiting the reduced-scale structures of cobblestone roads, was observed via the SEM images (Figure 1C) and the atomic force microscopy (AFM) images (Figure 1D) with an average Ra of 0.484 ± 0.037 nm (Figure S1), indicating the good smoothness of the coating. The energy dispersive x-ray (EDX) results also indicated a high level of element homogeneity of the coating (Figure S2), and the element content was

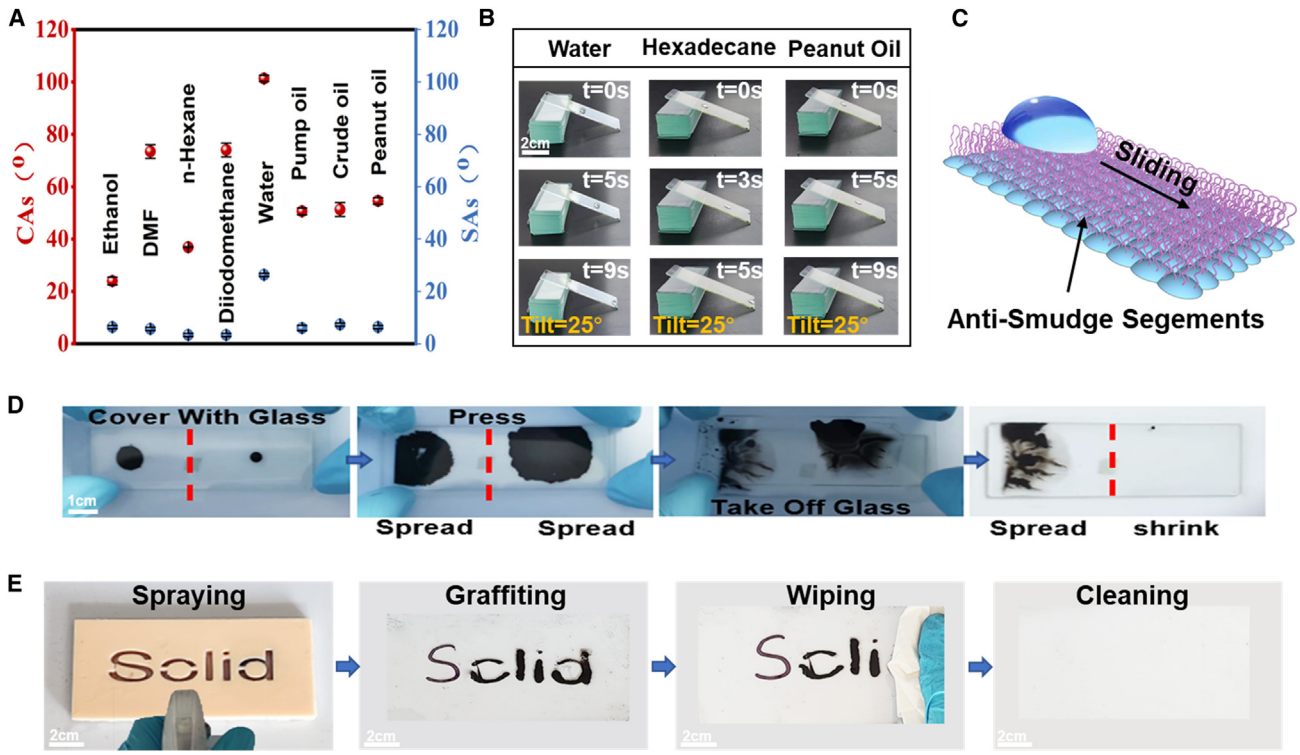

Figure 2. Good antifouling properties of the coating

(A) CAs and SAs of different liquids on the coating surfaces.

(B) Photographs of various liquids sliding off the coated glasses without leaving any residue.

(C) The image illustrating the liquid-like PDMS segments that anchor on the surface of the building blocks, thus achieving the anti-smudge surface function.

(D) The coating maintained its liquid repellency and anti-smudge performance when it was subjected to local pressure resulting from two pieces of squeezed glasses, tested with water-based ink.

(E) The sprayed oil-based graffiti can be readily wiped clean even via dry tissues.

further analyzed via X-ray photoelectron spectroscopy (XPS) (Figure S3). It is noteworthy that the curing temperature of coatings would initiate the remaining double bonds on the surfaces of building blocks thus obtaining the tense multi-crosslinking of the coating matrix. Furthermore, the spontaneous enrichment of the PDMS segments anchoring on the surface of the building blocks can create a low-surface-tension liquid-like monolayer for a long-lasting anti-smudge function. The transmittance of the coating was found to be above 98% in the entire testing range of 500–800 nm, and the insert picture of glass bearing the transparent coating does not obscure the vision (Figure 1E). This optical clarity would be attributed to the good distribution and sub-10 nm size of the building blocks, which are significantly smaller than the wavelength of visible light and would not cause undesirable scattering.[30,31] The chemicals and processes involved are readily available for the scalable preparation of this coating material.

Liquid repellency properties of the coating

To demonstrate the anti-smudge property of the coating, as shown in Figure 2A, the contact angles (CAs) and sliding angles (SAs) of various liquids with different surface tensions (including n-hexane, ethanol, *N, N*-Dimethylformamide (DMF), hexadecane, diiodomethane, and water with surface tensions of 20.3, 22.1, 25.7, 27.2, 50.8, and 72.8 mN/m at 20°C, respectively) and various oils with different viscosities (including peanut oil, pump oil, and crude oil with viscosities of ~80, 200, and 300 cP at 20°C, respectively) were evaluated. All these liquid droplets could easily slide off the coating surfaces, even with small CAs, which indicates the desired low adhesion and excellent anti-smudge performance of the coatings. Based on the CAs of water and n-hexadecane on the coated/uncoated surface, the surface energy of the coated surface was calculated to be approximately 22.72 mJ/m^2, largely smaller than that of the uncoated one (55.75 mJ/m^2) (see Table S1). Photographs in Figure 2B showed the processes of the water, hexadecane, and peanut oil sliding off the coating surfaces, these liquids would slide quickly without leaving any residue.

Lotus-inspired superhydrophobic or superoleophobic surfaces exhibiting liquid repellency rely on the entrapped air layer and surface topography and, thus would fail when in contact with pressured liquids as that tend to permutate into the textures and displace the air.[32–34] Unlike these pressure-sensitive rough surfaces, our coating was mainly attributed to the liquid-like anti-smudge segments that anchoring on the surface of the building blocks,[35,36] and the molecular functional surface is supposed to maintain its anti-smudge performance under pressure (Figure 2C). As shown in Figure 2D and Video S1, the ink

liquids were dropped both onto the uncoated and coated areas of the glass surface, and the other glass (also with uncoated and coated regions) was then placed on top and pressed down matching underneath to provide the local pressure. The spread liquid on the uncoated/coated glass interface exhibited different wetting phenomena when removing the top glass. It was observed that the droplets on the uncoated area spread out and were seriously stained, while the droplets on the coated interface shrank quickly and reverted back to smaller droplets. In contrast, if using an original glass to press, the liquid on the coating would be adhered to and carried away by the upper uncoated glass, leaving a clean coating surface without ink liquid, as shown in Figure S4. This indicates that when compared with the glass surface, the coating exhibited significantly lower adhesion properties. In addition, the coating exhibited easy clean properties toward undesired foreign materials such as graffiti. As shown in Figure 2E, when the oily inks of Sharpie markers are sprayed onto the coated glass, the graffiti can be easily removed even with the use of dry tissues. However, the oily ink traces on uncoated glass were difficult to remove (Figure S5).

Superhardness and good substrate adhesion of the coating

To enhance hardness is challenging for liquid repellency surfaces with different mechanisms including Lotus-inspired textures[37,38] and Nepenthes-inspired liquid films.[39,40] In contrast, the superhardness >9H at the inorganic level of our coating was determined according to the standard ASTM D3363 protocol.[41,42] The test indicated the highest pencil hardness rating of >9H, with unnoticeable scratches when the coating was subjected to the scratching using a 9H pencil with a load of 1 kg and the ink could still shrink on the scratched coating (Figure S6). This superhardness demonstrates superior performance compared to the commercial polyurethane (PU) coating, which exhibited a hardness (H) below the median score of the hardness scale (Figure S7). To avoid the impact of the substrates on the coatings, an indentation depth of 500 nm corresponding to less than 1% of the coating thickness (~60 μm, Figure S8) was used according to ISO 14577-4 standards.[43,44] Furthermore, the surface mechanical properties of the coating were further investigated via nanoindentation and nanoscratch tests (Figure S9). The nanohardness and elastic modulus values of the coating obtained as average values from five measurements were 368.7 MPa and 4.68 GPa, respectively, and the experimental values are listed in Table S2. For the wear test, the coating was abraded using steel wool under an average pressure of 15.0 kPa, and no peeling or scratches were observed on the coating surface after 200 abrasion cycles (Figure S10). Although the CAs and SAs of water and hexadecane were slightly changed after various abrasion cycles (Figure 3A), the droplets of these liquids were still able to slide off the coating surface without leaving any residual traces (Figure S11 and Video S2). The coating maintains anti-smudge properties after 1,000 cycles of abrasion when using cotton under an average pressure of 15.0 kPa Figure S12 shows the CAs and SAs of water and hexadecane after various abrasion cycles. Compared to other literature,[45–48] our coating exhibited well-combined features of antifouling, transmittance, and hardness, as shown in Figure S13.

The superhardness and excellent wear resistance mechanism of the anti-smudge surface are illustrated in Figure 3B. Just like we can only feel the hardness of stones when our footsteps on cobblestone roads, for this tensely crosslinked matrix comprised the sub-10 nm blocks, a micro- or nano-scaled tip should not be able to distinguish the blocks from the crosslinked interfaces. Thus, this coating would act as a continuous inorganic phase behavior when it is subjected to external forces with a contact point of above 10 nm length scale.

Contrary to the anti-smudge low adhesion surface of the coating, a strong adhesion bottom to substrates was achieved. As shown in Figure 3C, the shear strengths of the coating attached to a range of substrates were evaluated, including the tin plate, stainless steel (403), Al, and glass.[49] Among them, the coating on Al exhibited the lowest shear strength, which may be attributed to the highest thermal expansion coefficient of Al ($\sim 23.6 \times 10^{-6}/^{\circ}C$)[50] with significant surface expansion and shrinking changes. However, regardless of these substrates, a minimum shear strength higher than 200 kPa was achieved. This high level of adhesion could be attributed to the well-leveling and film-forming properties of the coating solution, resulting from the sub-10 nm composition and tense crosslinking chemistry. In addition, the chemical bonds could form between the hydroxyl group on the substrate surface and the residual silane agent of the coating. The hydroxyl and amino groups of the coating could form hydrogen interaction with the substrates. Thus, the coating is firmly attached to the metal substrate, and results in a strong adhesive bottom layer. The different shear strength values measured for various substrates can be ascribed to the varying substrate composition that resulted in different synergetic interfacial adhesion interactions between the coating materials and the substrates, e.g., hydrogen bonding, hydrophobic interactions, and van der Waals forces, etc.[51] Thus, the coating could be firmly attached to various hydrophilic and hydrophobic substrates, such as iron sheet, glass, porcelain, polylactic acid (PLA), and polytetrafluoroethylene (PTFE). A knife was used to create a hundred grid with an interval of 1 mm on the coating, and then adhered and peeled off via a 3M tape. The result showed that no species was peeled off after the adhesion strength test, indicating good adhesion between the coating and various substrates (Figure S14).

Corrosion resistance and good transparency

To determine the corrosion resistance of this coating, the half-coated steel sheet was subjected to various corrosive liquids, including $CuSO_4$ (1.0 mol/L), NaCl (1.0 mol/L), and HCl (1.0 mol/L). As shown in Figure 3D, the coated tin plate surface showed no signs of corrosion, while the uncoated area appeared to be seriously corroded. The anti-corrosion performances of a bare tin plate and a coated tin plate were further examined by an electrochemical corrosion test. As shown in Figure 3E and Figure S15, in comparison with the bare tin plate, the coated area exhibited a positive shift in the corrosion potential (Ecorr) and a reduction in the corrosion current density (Icorr). Generally, a higher Ecorr value and a lower corrosion Icorr value indicate that the coating provides better corrosion protection and is

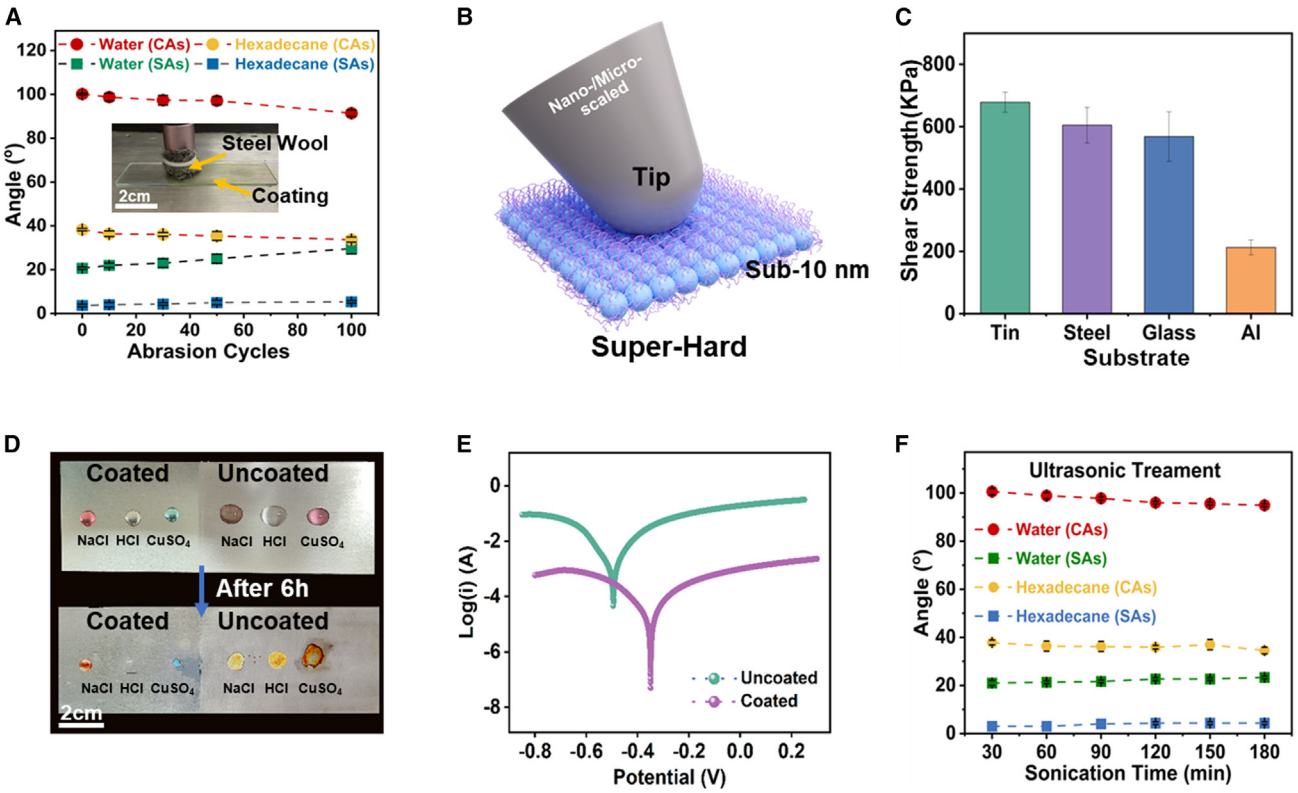

Figure 3. Good stability of the coatings

(A) The CAs and SAs of the coatings after abrasion using steel wool for various cycles.

(B) The illustration of the superhard mechanism of the anti-smudge surface when the coating is subjected to external forces. A micro- or nano-scale tip would not distinguish the sub-10 nm blocks and cause scratches.

(C) Shear strengths of coatings applied onto various substrates including metals and glass.

(D) The coated and uncoated steel for the corrosion protection tests at room temperature (~28°C), using HCl, $CuSO_4$, and NaCl solutions as corrosive liquids.

(E) Tafel polarization curves of bare and coated tin plates.

(F) The CAs and SAs of the coatings after the ultrasonic treatment (40 K Hz).

able to slow the dissolution rate of the substrate, which thus demonstrates that this coating imparts corrosion resistance.[52] Moreover, when the coating was immersed in various organic solvents (including n-hexane and *N, N*-dimethylacetamide (DMAC)), aqueous solutions with pH values ranging from 3 to 11, and artificial seawater for 21 days, the sliding behaviors of water and hexadecane on the coating surface were discovered negligible changes (Figures S16 and S17). In addition, the coating also maintained its liquid repellency after the treatment of underwater ultrasonic waves for 180 min (Figure 3F). These results confirmed that the coating is highly resistant to damage and has excellent durability for providing long-term protection of substrates.

It is noteworthy that the optical transparency of coating is important for the practical application of anti-smudge materials. Thus, this coating can be applied to the screen of electronic devices (e.g., smartphones) without changing its optical clarity (Figure 4A). The coating's repellency toward an artificial fingerprint liquid (consisting of lactic acid, acetic acid, sodium chloride, sodium hydrogen phosphate, 1-methoxy-2-propanol, hydroxyl-group-terminated polydimethylsiloxane, and deionized water) was investigated,[53] and an aqueous ink solution (1 wt %) was added to the artificial fingerprint liquid to present a clearer enlarged image of the trace that was pressed by a finger on the coated (Figure 4B) and uncoated (Figure S18) glass plates. The uncoated glass is readily wet and contaminated by the artificial fingerprint liquid. However, when this liquid is applied to the coated part, it contracts into distinct droplets immediately, and this contraction of the fingerprint would obviously weaken the disturbance toward reading.

This transparent coating could also find an application on the windscreen, as it repels liquid contaminations (Figure 4C and Video S3) as well as dust, which is readily carried away by rain (Figure S19). Remarkably, this coating can improve driving safety during rainy weather, as reducing raindrop retention can prevent rain-induced poor visibility. Sliding or staying of raindrops that splatter on the windscreen of a moving car is influenced by both gravity and the wind force.[54] To simulate this situation, we use a hair dryer to blow on the model windscreen with various volumes of water droplets, thus conducting a force analysis on the motion of the droplet, combined with Newton's second law "$F - f - mg\sin\alpha = ma$" (Figure 4D). The experimental results also indicated that the raindrops

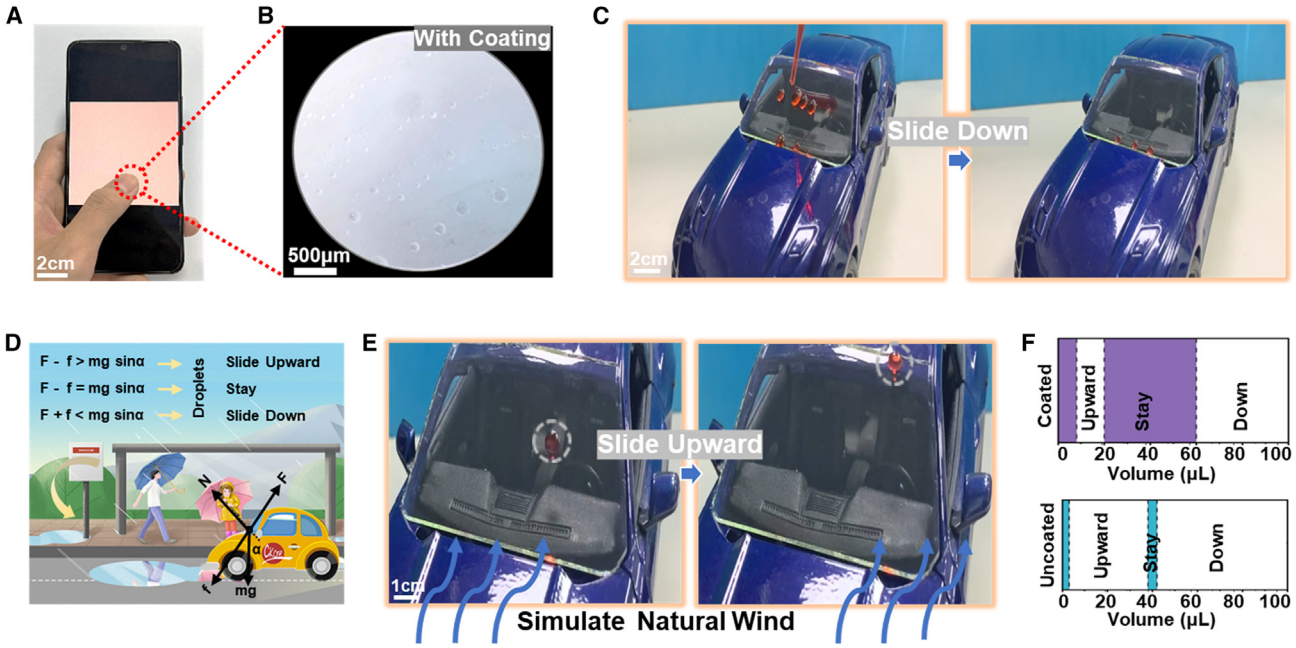

Figure 4. Potential application of the antifouling coatings

(A) The application of coating on the screen of a smartphone.

(B) The contraction of artificial fingerprint liquid on the coating surface after pressed by a finger, which were magnified via a microscope.

(C) The application of the coating on the car windscreen and the droplets would slide downward in natural surroundings.

(D) Force analysis of the raindrops on the windscreen, where "F," "f," "N," and "α" represents the wind force, resistance, supporting force, and the windscreen angles, respectively.

(E) The droplets would slide upward on a coated windscreen with wind conditions.

(F) Sliding movements of the liquids with different volumes.

were pulled down by gravity when the mess exceeded a certain threshold, while smaller ones were pushed upward when the wind prevailed (Figure 4E and Video S4). At both the sliding down and upward circumstances, the windscreen was clear without vision-disturbed residue. In contrast, medium-sized and very little droplets would stay as the difference between gravity and wind force could not overcome the friction, and these droplets would obstruct the driver's vision thus causing danger. Surprisingly, the volume range for droplets to stay was discovered to be very limited for the coated windscreen, while that is significantly larger for the uncoated glass. For a quantitative calculation according to the various liquid volumes, it was found that the liquid-solid contact fraction of the coating is only one-tenth of that of the uncoated glass.

Conclusion

In summary, we have created an anti-smudge coating with superhardness and high transparency via the nanoparticle pattern surface designing strategy of materials. Excellent repellency toward various liquids, hardness of above 9H, and transmittance of 98% were simultaneously achieved for this coating material. In addition, the chemicals and processes involved make this coating readily applied in large-area, daily, on-site applications on various substrates. The coating with combined properties is expected to have applications in fields including electronic screens and vehicle windows.

Limitations of the study

The limitation of this study is that the structure and roughness of the coating surface cannot be adjusted to prepare series patterns.

RESOURCE AVAILABILITY

Lead contact

Further information and requests for resources and reagents should be directed to the lead contact, Xiubin Xu (xuxb@gzhu.edu.cn).

Materials availability

This study did not generate new unique reagents.

Data and code availability

- All data reported in this paper will be shared by the lead contact upon request.
- This paper does not report the original code.
- Any additional information required to reanalyze the data reported in this paper is available from the lead contact upon request.

ACKNOWLEDGMENTS

We wish to thank the National Natural Science Foundation of China (22278093 and 22108049), Guangdong Basic and Applied Basic Research Foundation (2023B1515020092 and 2024A1515011240), the Science and Technology Project of Guangdong Province of China (2023A0505050095), and the Science and Technology Project of Guangzhou City (2023A03J0031 and 2024A04J3276) for sponsoring this research. We would like to thank the

Analysis and Test Center of Guangzhou University for their assistance with the characterizations.

AUTHOR CONTRIBUTIONS

Conceptualization, X.X. and X.W.; investigation, J.L. and D.L.; formal analysis, J.L., X.X., D.L., Y.L., Y.H., and X.W.; visualization, J.L., D.L., Y.L., and Y.H.; writing – original draft, review & editing, X.X. and X.W.; funding acquisition, X.X. and X.W., supervision, X.X. and X.W.

DECLARATION OF INTERESTS

The authors declare no competing interests.

STAR★METHODS

Detailed methods are provided in the online version of this paper and include the following:

- KEY RESOURCES TABLE
- METHOD DETAILS
  - Characterization and measurements
  - Preparation of the coating
- QUANTIFICATION AND STATISTICAL ANALYSIS

SUPPLEMENTAL INFORMATION

Supplemental information can be found online at https://doi.org/10.1016/j.isci.2025.111996.

Received: September 4, 2024
Revised: November 12, 2024
Accepted: February 7, 2025
Published: February 12, 2025

REFERENCES

1. Tuteja, A., Choi, W., Ma, M., Mabry, J.M., Mazzella, S.A., Rutledge, G.C., McKinley, G.H., and Cohen, R.E. (2007). Designing superoleophobic surfaces. Science *318*, 1618–1622.
2. Wong, T.-S., Kang, S.H., Tang, S.K.Y., Smythe, E.J., Hatton, B.D., Grinthal, A., and Aizenberg, J. (2011). Bioinspired self-repairing slippery surfaces with pressure-stable omniphobicity. Nature *477*, 443–447. https://doi.org/10.1038/nature10447.
3. Deng, X., Mammen, L., Butt, H.-J., and Vollmer, D. (2012). Candle Soot as a Template for a Transparent Robust Superamphiphobic Coating. Science *335*, 67–70. https://doi.org/10.1126/science.1207115.
4. Liu, T.L., and Kim, C.J.C.J. (2014). Turning a surface superrepellent even to completely wetting liquids. Science *346*, 1096–1100. https://doi.org/10.1126/science.1254787.
5. Yao, L., Sathasivam, S., Song, J., Crick, C.R., Carmalt, C.J., and Parkin, I.P. (2015). Robust self-cleaning surfaces that function when exposed to either air or oil. Science *347*, 1132–1135. https://doi.org/10.1126/science.aaa4298.
6. Liu, Y., Ma, J., Yang, Y., Valenzuela, C., Zhang, X., Wang, L., and Feng, W. (2024). Smart chiral liquid crystal elastomers: Design, properties and application. Smart Molecules *2*, e20230025. https://doi.org/10.1002/smo.20230025.
7. Schmidt, D.L., Coburn, C.E., Dekoven, B.M., Potter, G.E., Meyers, G.F., and Fischer, D.A. (1994). Water-based non-stick hydrophobic coatings. Nature *368*, 39–41. https://doi.org/10.1038/368039a0.
8. Liu, M., Wang, S., and Jiang, L. (2017). Nature-inspired superwettability systems. Nat. Rev. Mater. *2*, 17036. https://doi.org/10.1038/natrevmats.2017.36.
9. Buddingh, J.V., Hozumi, A., and Liu, G. (2021). Liquid and liquid-like surfaces/coatings that readily slide fluids. Prog. Polym. Sci. *123*, 101468. https://doi.org/10.1016/j.progpolymsci.2021.101468.
10. Zhong, X.-M., Wyman, I., Yang, H., Wang, J.-B., and Wu, X. (2016). Preparation of robust anti-smudge coatings via electrophoretic deposition. Chem. Eng. J. *302*, 744–751. https://doi.org/10.1016/j.cej.2016.05.112.
11. Cai, X., Wang, X., Bian, F., Li, J., Zhou, R., Hu, J., and Lin, S. (2024). Flexible sensor based on conformable, sticky, transparent elastomers for electronic skin. Chem. Eng. J. *498*, 154934. https://doi.org/10.1016/j.cej.2024.154934.
12. Wang, D., Sun, Q., Hokkanen, M.J., Zhang, C., Lin, F.-Y., Liu, Q., Zhu, S.-P., Zhou, T., Chang, Q., He, B., et al. (2020). Design of robust superhydrophobic surfaces. Nature *582*, 55–59. https://doi.org/10.1038/s41586-020-2331-8.
13. Tian, X., Verho, T., and Ras, R.H.A. (2016). Moving superhydrophobic surfaces toward real-world applications. Science *352*, 142–143. https://doi.org/10.1126/science.aaf2073.
14. Dhyani, A., Wang, J., Halvey, A.K., Macdonald, B., Mehta, G., and Tuteja, A. (2021). Design and applications of surfaces that control the accretion of matter. Science *373*, eaba5010. https://doi.org/10.1126/science.aba5010.
15. Chen, H., Wang, F., Fan, H., Hong, R., and Li, W. (2021). Construction of MOF-based superhydrophobic composite coating with excellent abrasion resistance and durability for self-cleaning, corrosion resistance, anti-icing, and loading-increasing research. Chem. Eng. J. *408*, 127343. https://doi.org/10.1016/j.cej.2020.127343.
16. Clément Sanchez, P.B., Belleville, P., Popall, M., and Nicole, L. (2011). Applications of advanced hybrid organic–inorganic nanomaterials from laboratory to market. Chem. Soc. Rev. *40*, 696–753. https://doi.org/10.1039/C0CS00136H.
17. Mammeri, F., Bourhis, E.L., Rozes, L., and Sanchez, C. (2005). Mechanical properties of hybrid organic–inorganic materials. J. Mater. Chem. *15*, 3787. https://doi.org/10.1039/b507309j.
18. Qi, Y., and Zhang, S. (2023). Recent progress in low-swellable polymer-based smart photonic crystal sensors. Smart Molecules *1*, e20230018. https://doi.org/10.1002/smo.20230018.
19. Hu, X., Tang, C., He, Z., Shao, H., Xu, K., Mei, J., and Lau, W.M. (2017). Highly Stretchable Superhydrophobic Composite Coating Based on Self-Adaptive Deformation of Hierarchical Structures. Small *13*, 1602353. https://doi.org/10.1002/smll.201602353.
20. Wang, S., Yu, X., and Zhang, Y. (2017). Large-scale fabrication of translucent, stretchable and durable superhydrophobic composite films. J. Mater. Chem. A Mater. *5*, 23489–23496. https://doi.org/10.1039/c7ta08203g.
21. Davis, A., Surdo, S., Caputo, G., Bayer, I.S., and Athanassiou, A. (2018). Environmentally Benign Production of Stretchable and Robust Superhydrophobic Silicone Monoliths. ACS Appl. Mater. Interfaces *10*, 2907–2917. https://doi.org/10.1021/acsami.7b15088.
22. Yao, X., Hu, Y., Grinthal, A., Wong, T.-S., Mahadevan, L., and Aizenberg, J. (2013). Adaptive fluid-infused porous films with tunable transparency and wettability. Nat. Mater. *12*, 529–534. https://doi.org/10.1038/nmat3598.
23. Uehara, H., Yamanobe, T., Yukawa, Y., and Matsuoka, Y. (1990). Method of Manufacture of Polytetrafluoroethylene Stretched Film, and Polytetrafluoroethylene Stretched Film. U.S. Patent. USPCT US90, 01236.
24. Bodö, P., and Schott, M. (1996). Highly Oriented Polytetrafluoroethylene Films A Force Microscopy Study. Thin Solid Films *286*, 98–106. https://doi.org/10.1016/S0040-6090(95)08529-7.
25. Zhang, K., Huang, S., Wang, J., and Liu, G. (2019). Transparent Omniphobic Coating with Glass-Like Wear Resistance and Polymer-Like Bendability. Angew Chem. Int. Ed. Engl. *58*, 12004–12009. https://doi.org/10.1002/anie.201904210.
26. Bender, D.N., Zhang, K., Wang, J., and Liu, G. (2021). Hard yet Flexible Transparent Omniphobic GPOSS Coatings Modified with Perfluorinated

Agents. ACS Appl. Mater. Interfaces *13*, 10467–10479. https://doi.org/10.1021/acsami.0c23151.

27. Zhang, K., Huang, S., Wang, J., and Liu, G. (2020). Transparent organic/silica nanocomposite coating that is flexible, omniphobic, and harder than a 9H pencil. Chem. Eng. J. *396*, 125211. https://doi.org/10.1016/j.cej.2020.125211.
28. Chen, F., Lin, F., Zhang, Q., Cai, R., Wu, Y., and Ma, X. (2019). Polyhedral Oligomeric Silsesquioxane Hybrid Polymers: Well-Defined Architectural Design and Potential Functional Applications. Macromol. Rapid Commun. *40*, e1900101. https://doi.org/10.1002/marc.201900101.
29. Kuo, S.-W., and Chang, F.-C. (2011). POSS related polymer nanocomposites. Prog. Polym. Sci. *36*, 1649–1696. https://doi.org/10.1016/j.progpolymsci.2011.05.002.
30. Chen, J., Zhong, X., Lin, J., Wyman, I., Zhang, G., Yang, H., Wang, J., Wu, J., and Wu, X. (2016). The facile preparation of self-cleaning fabrics. Compos. Sci. Technol. *122*, 1–9. https://doi.org/10.1016/j.compscitech.2015.11.015.
31. Wu, X., Wyman, I., Zhang, G., Lin, J., Liu, Z., Wang, Y., and Hu, H. (2016). Preparation of superamphiphobic polymer-based coatings via spray- and dip-coating strategies. Prog. Org. Coating *90*, 463–471. https://doi.org/10.1016/j.porgcoat.2015.08.008.
32. Nguyen, T.P.N., Brunet, P., Coffinier, Y., and Boukherroub, R. (2010). Quantitative Testing of Robustness on Superomniphobic Surfaces by Drop Impact. Langmuir *26*, 18369–18373. https://doi.org/10.1021/la103097y.
33. Bocquet, L., and Lauga, E. (2011). A smooth future? Nat. Mater. *10*, 334–337. https://doi.org/10.1038/nmat2994.
34. Poetes, R., Holtzmann, K., Franze, K., and Steiner, U. (2010). Metastable Underwater Superhydrophobicity. Phys. Rev. Lett. *105*, 166104. https://doi.org/10.1103/PhysRevLett.105.166104.
35. Amini, S., Kolle, S., Petrone, L., Ahanotu, O., Sunny, S., Sutanto, C.N., Hoon, S., Cohen, L., Weaver, J.C., Aizenberg, J., et al. (2017). Preventing mussel adhesion using lubricant-infused materials. Science *357*, 668–673. https://doi.org/10.1126/science.aai8977.
36. Liu, M., Liu, P., Wang, Z., Yao, H., Yao, X., and Wang, Z. (2019). Supramolecular silicone coating capable of strong substrate bonding, readily damage healing, and easy oil sliding. Sci. Adv. *5*, eaaw5643. https://doi.org/10.1126/sciadv.aaw5643.
37. Chen, F., Wang, Y., Tian, Y., Zhang, D., Song, J., Crick, C.R., Carmalt, C.J., Parkin, I.P., and Lu, Y. (2022). Robust and durable liquid-repellent surfaces. Chem. Soc. Rev. *51*, 8476–8583. https://doi.org/10.1039/d0cs01033b.
38. Zhang, W., Wang, D., Sun, Z., Song, J., and Deng, X. (2021). Robust superhydrophobicity: mechanisms and strategies. Chem. Soc. Rev. *50*, 4031–4061. https://doi.org/10.1039/D0CS00751J.
39. Hou, X., Zhang, Y.S., Santiago, G.T.-d., Alvarez, M.M., Ribas, J., Jonas, S.J., Weiss, P.S., Andrews, A.M., Aizenberg, J., and Khademhosseini, A. (2017). Interplay between materials and microfluidics. Nat. Rev. Mater. *2*, 17016. https://doi.org/10.1038/natrevmats.2017.16.
40. Grinthal, A., and Aizenberg, J. (2014). Mobile Interfaces: Liquids as a Perfect Structural Material for Multifunctional, Antifouling Surfaces. Chem. Mater. *26*, 698–708. https://doi.org/10.1021/cm402364d.
41. Wu, X., Liu, M., Zhong, X., Liu, G., Wyman, I., Wang, Z., Wu, Y., Yang, H., and Wang, J. (2017). Smooth Water-Based Antismudge Coatings for Various Substrates. ACS Sustain. Chem. Eng. *5*, 2605–2613. https://doi.org/10.1021/acssuschemeng.6b02957.
42. Pedraza, E.P., and Soucek, M.D. (2005). Effect of functional monomer on the stability and film properties of thermosetting core–shell latexes. Polymer *46*, 11174–11185. https://doi.org/10.1016/j.polymer.2005.08.069.
43. Lofaj, F., Ferdinandy, M., Cempura, G., and Dusza, J. (2012). Nanoindentation, AFM and tribological properties of thin nc-WC/a-C Coatings. J. Eur. Ceram. Soc. *32*, 2043–2051. https://doi.org/10.1016/j.jeurceramsoc.2012.01.037.
44. Gao, S., Gao, S., Xu, B., and Yu, H. (2015). Effects of Different pH-Values on the Nanomechanical Surface Properties of PEEK and CFR-PEEK Compared to Dental Resin-Based Materials. Materials *8*, 4751–4767. https://doi.org/10.3390/ma8084751.
45. Zhou, M., Ha, Z., Lei, L., Xia, Y., Mao, P., Chen, X., Fan, B., and Shi, S. (2022). Castor oil-based transparent and omniphobic polyurethane coatings with high hardness, anti-smudge and anti-corrosive properties. Prog. Org. Coating *172*, 107120. https://doi.org/10.1016/j.porgcoat.2022.107120.
46. Guo, G., You, T., Yang, X., and Li, W. (2024). Ultraviolet-cured polyurea-polyurethane acrylate/polysiloxane hybrid anti-fouling coatings with superior mechanical properties, transparency, and durability. Prog. Org. Coating *197*, 108832. https://doi.org/10.1016/j.porgcoat.2024.108832.
47. Fu, K., Tian, Y., Zhu, Z., Fa, S., and Zhang, Q. (2023). Highly-transparent fluorinated epoxy coating prepared via ring-opening of thiolactone and thiol-click reactions for robust omniphobicity. Prog. Org. Coating *179*, 107519. https://doi.org/10.1016/j.porgcoat.2023.107519.
48. Gao, P., Wang, Y., Wang, J., Wang, F., Ma, W., Zhang, Z., Men, X., and Lu, Y. (2022). Rational Design of Durable Anti-fouling Coatings with High Transparency, Hardness, and Flexibility. ACS Appl. Mater. Interfaces *14*, 29156–29166. https://doi.org/10.1021/acsami.2c04279.
49. Chen, R., Xu, X., Yu, D., Liu, M., Xiao, C., Wyman, I., Wang, Z., Yang, H., and Wu, X. (2019). Temperature-regulated flexibility of polymer chains in rapidly self-healing hydrogels. NPG Asia Mater. *11*, 22. https://doi.org/10.1038/s41427-019-0123-0.
50. Nyanor, P., El-Kady, O., Yehia, H.M., Hamada, A.S., and Hassan, M.A. (2021). Effect of Bimodal-Sized Hybrid TiC–CNT Reinforcement on the Mechanical Properties and Coefficient of Thermal Expansion of Aluminium Matrix Composites. Met. Mater. Int. *27*, 753–766. https://doi.org/10.1007/s12540-020-00802-w.
51. Yu, D., Huang, J., Zhang, Z., Weng, J., Xu, X., Zhang, G., Zhang, J., Wu, X., Johnson, M., Lyu, J., et al. (2022). Simultaneous Realization of Superoleophobicity and Strong Substrate Adhesion in Water via a Unique Segment Orientation Mechanism. Adv. Mater. *34*, 2106908. https://doi.org/10.1002/adma.202106908.
52. Nine, M.J., Cole, M.A., Johnson, L., Tran, D.N.H., and Losic, D. (2015). Robust Superhydrophobic Graphene-Based Composite Coatings with Self-Cleaning and Corrosion Barrier Properties. ACS Appl. Mater. Interfaces *7*, 28482–28493. https://doi.org/10.1021/acsami.5b09611.
53. Wu, L.Y., Ngian, S.K., Chen, Z., and Xuan, D.T.T. (2011). Quantitative test method for evaluation of anti-fingerprint property of coated surfaces. Appl. Surf. Sci. *257*, 2965–2969. https://doi.org/10.1016/j.apsusc.2010.10.101.
54. Hooshanginejad, A., and Lee, S. (2022). Dynamics of a partially wetting droplet under wind and gravity. Phys. Rev. Fluids *7*, 033601. https://doi.org/10.1103/PhysRevFluids.7.033601.

STAR★METHODS

KEY RESOURCES TABLE

REAGENT or RESOURCE	SOURCE	IDENTIFIER
Amino-terminated polydimethylsiloxane	Suzhou Qitian New Materials	CAS: 63148-62-0
(3-Aminopropyl) triethoxysilane	Macklin	CAS: 919-30-2
Pentaerythritol triacrylate	Macklin	CAS: 3524-68-3
Ethanol	Macklin	CAS: 64-17-5
Diiodomethane	Macklin	CAS: 75-11-6
n-Hexane	Macklin	CAS: 110-54-3
Dimethylacetamide	Macklin	CAS: 617-84-5
2-Acetoxymethyl-1-Methoxypropane	Macklin	CAS: 116-11-0
Hexadecane	Macklin	CAS: 544-76-3
Commercial polyurethane	Macklin	N/A
Light crude oil	PetroChina	N/A
HCl	Tianjin Damao	CAS: 7647-01-0
NaCl	Tianjin Damao	CAS: 7757-82-6
NaOH	Tianjin Damao	CAS: 1310-73-2
Peanut oil	local stores	N/A
Pump oil	local stores	N/A

METHOD DETAILS

Characterization and measurements

The size distribution of building blocks was measured by Malvern Zetasizer Nano ZS90, and all the tests were performed in triplicate. The CAs and SAs were measured using a CA measuring instrument (JC2000A). The droplet volumes employed in the CAs and SAs measurements were 5 and 20 μL. Transmittance spectra of the coating were measured from 450 to 800 nm using a UV-visible spectrometer (Varian Cary 7000 spectrophotometer) with bare glass as a reference. Scanning electron microscopy (SEM) images of coatings were obtained by a Zeiss Sigma 300 scanning electron microscope at 5 kV. Coatings were sputtered with gold via Quorum SC7620 before SEM observations, and the elemental content was obtained by EDX characterization. AFM images of coatings were obtained by a Bruker Dimension Iconscanning probe microscope. XPS (K-Alpha, Thermo Fisher Scientific) equipped with monochromatized Al Kα radiation (hυ = 1486.7 eV) was employed to analyze the elemental composition of the coating surface. The pencil hardness of the coating was determined using a VF2378 pencil hardness tester (Thermimport Quality Control, Netherlands). The final pencil hardness of the coating is equal to the pencil that was just soft enough for not being able to make scratches on a coating. Abrasion tests were measured by an abrasion test system (Chuangheng, A20-339) with a piece of steel wool as the abrasion material, using a weight of 500 g placed above to enhance the abrasion force. Nanoindentation tests were measured by a nanoindentor (Bruker Hysitron TI980) equipped with a Berkovich diamond tip at 25°C. For each force loading, holding, and unloading cycle, the maximum load was 500 μN, and the loading and unloading rates were both at 100 μN/s. The nanoindentation hardness and effective Young's moduli were calculated by computer using the OliverPharr method. For the substrate adhesion tests, the coating solution was applied to the substrate, and then covered with another substrate slide, and subsequently cured to obtain the test samples. The samples were evaluated using a universal testing machine (HZ-1007E, Dongguan Lixian Instrument Technology Co., Ltd) at a rate of 50 mm min^{-1}. A pulling force was applied to the samples until a separation occurred between the coating and the substrate, then the maximum stress and strain values were recorded. The shear strength was determined as the ratio of the maximum stress and the coating area. At least five parallel samples were tested for each group.

Preparation of the coating

20.0 g APTES was dissolved in 2.0 g deionized water and 20.0 g ethanol, and the mixture was subsequently stirred for 4 h at 60°C to prepare the mixture A. PETA (3.0 g), ethanol (1.0 g), and PMA (1.0 g) were stirred thoroughly at 400 rpm and room temperature (ca. 25°C) in a sealed container for 10 min to prepare the mixture B. Subsequently, NH_2-PDMS-NH_2 (0.1 g) and the mixture A

(1.2 g) were slowly added into the mixture B and stirred at 400 rpm and room temperature (ca. 25°C) for 24 h to obtain the clear solution. This solution was casted onto substrates including glass and tin plate, and the desired coating materials were prepared after a simple thermal curing process at 180°C for 2h.

QUANTIFICATION AND STATISTICAL ANALYSIS

Averaged values and standard deviation (s. d.) are calculated from at least 3 different measurements for each entry. The quantitative data were presented as mean ± standard deviation.